Available online at www.sciencedirect.com
SCIENCE DIRECT®
Thin Solid Films 446 (2004) 18–22
www.elsevier.com/locate/tsf

Epitaxial growth of anatase by reactive sputter deposition using water vapor as the oxidant

B.-S. Jeong[a], D.P. Norton[a,*], J.D. Budai[b], G.E. Jellison[b]

[a]University of Florida, Department of Materials Science and Engineering, 106 Rhines Hall, Gainesville, FL 32611, USA
[b]Oak Ridge National Laboratory, Solid State Division, Oak Ridge, TN 37831, USA

Received 18 December 2002; received in revised form 13 August 2003; accepted 26 August 2003

Abstract

The growth of TiO_2 films in the anatase crystal structure was investigated using reactive sputter deposition with H_2O serving as the oxidizing species. With water vapor, the formation of phase-pure anatase TiO_2 thin films via epitaxial stabilization on (001) $LaAlO_3$ was achieved, although crystallinity was slightly inferior to that obtained when O_2 was employed. Films grown using water vapor exhibited a rougher surface morphology indicating a difference in growth mechanisms. At low H_2O pressure, the formation of a Ti_nO_{2n-1} Magnéli phase was observed. When hydrogen was employed during growth, mixed phase films of rutile and anatase resulted. The development of crystallinity and phase as a function of deposition temperature and oxidant pressure are discussed.
© 2003 Elsevier B.V. All rights reserved.

Keywords: Epitaxy; Oxides; Semiconductors; Titanium oxide

1. Introduction

In recent years, there has emerged significant interest in the synthesis of TiO_2 thin films. Wide bandgap semiconducting oxides, such as TiO_2, are useful for a number of applications, including transparent conducting oxides [1], chemical sensors [2–5], and optical components. TiO_2 occurs in three distinct polymorphs, namely rutile, anatase, and brookite. Anatase and rutile have the same symmetry, tetragonal 4/m 2/m 2/m, despite having different structures. In rutile, the structure is based on octahedra of titanium oxide that share two edges of the octahedron with other octahedrons and form chains. It is the chains themselves that are arranged into a four-fold symmetry. In anatase, the octahedrons share four edges hence the four-fold axis. Rutile is the thermodynamically stable phase at high temperatures, and is the most widely studied. In polycrystalline films, rutile is the more common phase observed. Limited work has been done on brookite, which is orthorhombic with 2/m 2/m 2/m symmetry [6]. Anatase is a metastable polymorph that can be realized in polycrystalline films deposited at low temperatures [7–11]. Despite being metastable, single crystals of anatase have been realized via chemical transport reaction processes [12,13]. Undoped anatase is an anisotropic, tetragonal insulator ($a=3.78$ Å, $c=9.52$ Å) with a bandgap of 3.2 eV [14]. The static dielectric constant of anatase is reported as 31 [15]. TiO_2 can be made an n-type semiconductor with $n\sim10^{19}/cm^3$ via chemical substitution or by Ti interstitials [16–19]. Low temperature electron Hall mobility on the order of 30–100 cm^2/V s has been reported for rutile. Hall mobility of n-type anatase has been measured as high as 20 cm^2/V s.

There is significant interest in the synthesis of phase-pure anatase thin films, both for applications and fundamental studies. In catalysis, photocatalysis, and dye-sensitized solar cells, anatase has proven advantageous over the rutile phase [20–23]. Controlling the electronic properties, surface structure, and morphology are key elements in these applications. Recently, it has been reported that transition metal doped semiconducting anatase can be ferromagnetic at room temperature [24]. This is of significant interest in the development of spin-based electronics. As the mechanism for ferro-

*Corresponding author. Tel.: +1-352-846-0525; fax: +1-352-846-1182.
E-mail address: dnort@mse.ufl.edu (D.P. Norton).

0040-6090/04/$ - see front matter © 2003 Elsevier B.V. All rights reserved.
doi:10.1016/S0040-6090(03)01238-0

magnetism may be carrier-mediated, there is interest in manipulating carrier density in epitaxial anatase films. In addition, the realization of spin-based electronic devices requires atomic-scale control of surfaces and interfaces. Numerous efforts have focused on the formation of anatase films that are phase pure and highly crystalline [15,25–34]. In general, epitaxial stabilization offers a means by which anatase thin films can be obtained on lattice-matched substrates, often for processing conditions where the phase is thermodynamically unstable in bulk. Understanding how growth conditions impact phase development, film morphology, and crystallinity is important in exploring these applications.

In this paper, we report on the synthesis and properties of epitaxial anatase, focusing on the use of water vapor as the oxidizing species during reactive sputter deposition. In particular, we have investigated the use of H_2O and H_2O/H_2 in the growth of anatase films. Previous work reporting highly crystalline anatase films via reactive sputter deposition focused on the use of oxygen [35]. The introduction of hydrogen-bearing species into the growth process produces the potential to modify the Ti valence state, thus introducing charge carriers. Here, we address the phase development, crystallinity, and surface morphology of anatase as a function of oxidizing species, oxidation conditions, and temperature using reactive sputter deposition.

2. Experimental details

The film growth experiments were performed in a reactive radio frequency (RF) magnetron sputter deposition system equipped with a load-lock for substrate exchange. A quartz lamp heater provided for substrate heating up to 750 °C. Two-inch diameter Ti sputtering targets were used. The target-to-substrate distance was approximately 15 cm. The base pressure of the deposition system was on the order of 5×10^{-8} Torr. For epitaxially stabilized anatase film growth, (001) $LaAlO_3$ was chosen as the substrate as it provides a lattice mismatch on the order of 0.2%. For comparison, Si substrates were also used so as to produce polycrystalline films under the same conditions. The substrates were cleaned in trichloroethylene, acetone and ethanol prior to mounting on the sample platen with Ag paint. The oxygen was provided through a mass flow control valve. A water source was created by freezing and evacuating a water-filled stainless steel cylinder that was attached to the deposition chamber via a leak valve. Upon returning to room temperature, the vapor pressure of water is sufficient to provide an H_2O source. As mentioned before, the use of water vapor and hydrogen in depositing oxide materials is useful in manipulating the valence of cations in the depositing film. The presence of hydrogen during deposition can result in oxygen deficiency and semiconducting behavior. Structure of the film was determined using X-ray diffraction via a Cu K-α source. Surface morphology was determined using a Nanoscope II instrument. Transport properties of oxygen-deficient TiO_2 anatase films will be reported elsewhere.

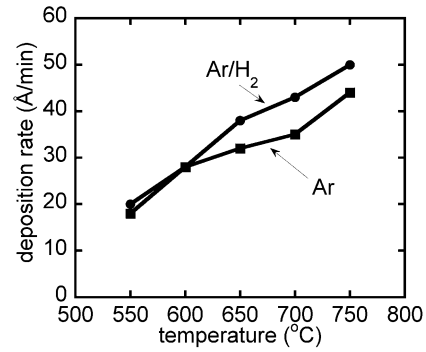

Fig. 1. Deposition rate of TiO_2 films on $LaAlO_3$ as a function of substrate temperature, with H_2O serving as the oxidizing species.

3. Results and discussion

For films deposited using water vapor, anatase was obtained with comparable deposition rate, but slightly inferior crystallinity, as compared to that achieved with O_2. The epitaxial relationship between the film and substrate, as determined by four-circle X-ray diffraction, was $(001)[110]_{LaAlO3}//(001)[110]_{anatase}$, as has been reported elsewhere [35,36]. The deposition rate for TiO_2 showed a slight dependence on substrate temperature as is shown in Fig. 1. Growth rate was determined measuring the final film thickness across a step using a surface profilometer. The rates are for an applied RF power of 250 W, $P(H_2O)=10^{-3}$ Torr, and a total pressure of 15 mTorr. The background gas was either argon or a 4% H_2/96% Ar mixture. The deposition rate did not change significantly when oxygen was used in place of water vapor. The increase in deposition rate with temperature reflects the limiting surface reaction of Ti with the oxidizing species to yield TiO_2, since the sticking coefficient of Ti should be near unity. For most of the films discussed below, the deposition time was 2 h, yielding a film thickness on the order of 350 nm.

The effectiveness of epitaxy in stabilizing the anatase crystal structure can be seen in Figs. 2 and 3, where the X-ray diffraction patterns for TiO_2 films deposited at various temperatures on either $LaAlO_3$ or Si are shown. For these films, the total pressure during deposition was 15 mTorr, with 10^{-3} Torr of H_2O vapor pressure. For films deposited at a substrate temperature ranging from 500 to 750 °C, the dominant TiO_2 phase observed on (001) $LaAlO_3$ was (001)-oriented anatase. Fig. 4a shows the X-ray diffraction intensity as a function of deposition temperature for the anatase (004) peak. The films

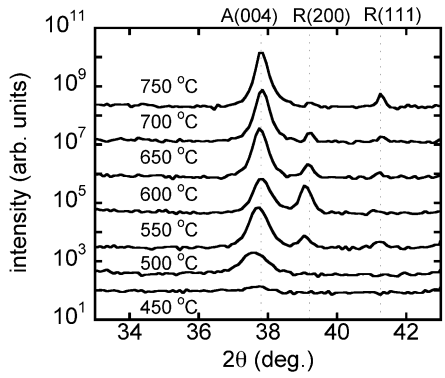

Fig. 2. X-Ray diffraction patterns for TiO_2 films deposited at an Ar pressure of 15 mTorr and a water vapor partial pressure of 10^{-3} Torr on $LaAlO_3$.

deposited at the higher temperatures possess a c-axis lattice parameter that is essentially the same as bulk crystals. However, at the lower growth temperatures, there is a distinguishable shift to longer lattice spacing for both the anatase and rutile components, indicating a defect structure. Plotted in Fig. 4b are the relative ratios of the (004) anatase peak to the (200) and (111) rutile peaks. Anatase is clearly the dominant TiO_2 phase with the strongest relative (004) anatase peak at a growth temperature of 750 °C. In contrast, the diffraction data for polycrystalline TiO_2 films deposited on silicon substrates are predominantly rutile, particularly at the elevated temperatures, with only a minority anatase component present. The exceptions to this are the films deposited at $T \leq 500$ °C, where the crystallinity is poor and the anatase structure appears more prominent. Clearly, the epitaxial nucleation of TiO_2 on a lattice-matched substrate provides a robust processing window for realizing anatase phase selection and crystallinity.

Epitaxy of the films with respect to the substrate was examined using four-circle X-ray diffraction. A low-resolution θ–2θ scan along the TiO_2 (001) shows that

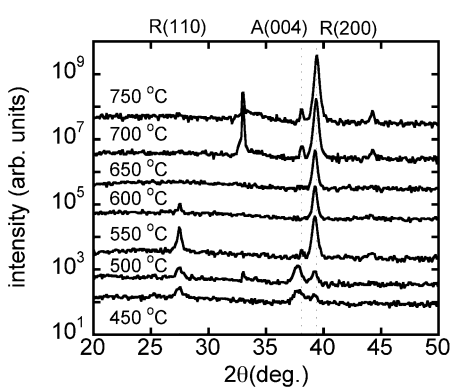

Fig. 3. X-Ray diffraction patterns for TiO_2 films deposited at an Ar pressure of 15 mTorr and a water vapor partial pressure of 10^{-3} Torr on Si.

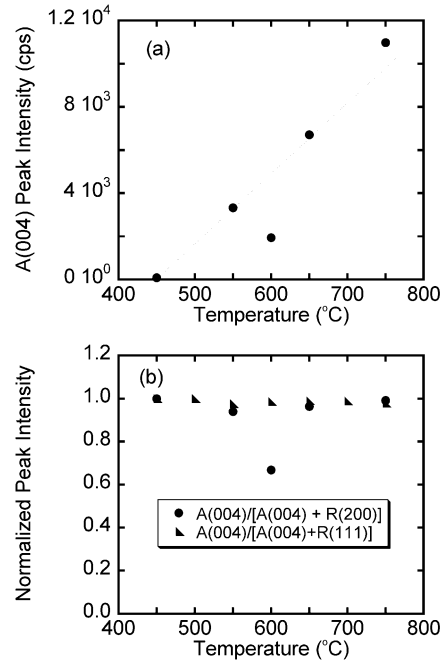

Fig. 4. X-Ray diffraction data for TiO_2 on $LaAlO_3$ using H_2O. Shown are (a) the anatase (004) peak intensity and (b) the relative intensity of anatase peaks to the rutile peaks.

the predominant phase is (001) anatase, although some minor peaks attributable to rutile are evident. From a high-resolution θ–2θ scan through the anatase (004), the lattice parameters for the anatase film deposited at 700 °C and 10^{-3} Torr of H_2O are determined to be $a = b = 3.78$ Å, $c = 9.522$ Å, which is essentially that reported for bulk material. A θ-scan rocking curve through the (004) yields a $\Delta\theta = 0.58°$ full-width-half-maximum. Fig. 5 shows the f-scan through the anatase {204)} peaks showing that the film is in-plane aligned. The $\Delta\varphi$ full-width half-maximum (FWHM) for the in-plane peaks is 0.6°. The in-plane and out-of-plane mosaic widths for anatase grown using water vapor are some-

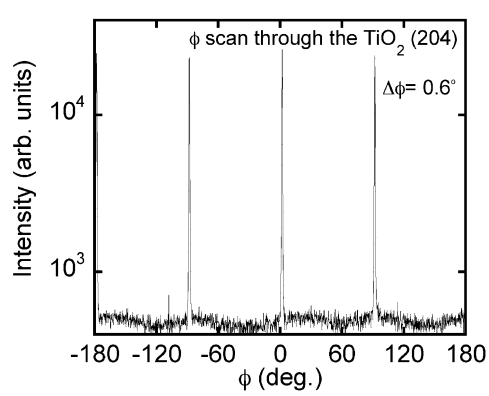

Fig. 5. The φ–scan through the anatase {204} peaks, showing in-plane alignment for the films grown using H_2O.

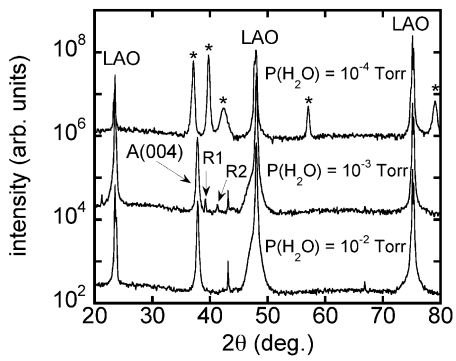

Fig. 6. The X-ray diffraction patterns for films deposited with 15 mTorr Ar (no hydrogen) as a function of water vapor pressure. The anatase (A) and rutile peaks are indicated, with R1 = rutile (200) and R2 = rutile (111). The asterisks indicate the Magnéli phase peaks.

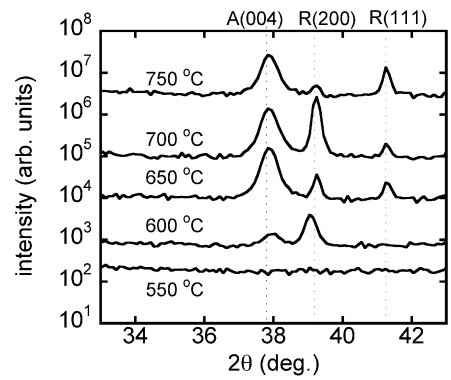

Fig. 7. X-Ray diffraction patterns for TiO_2 films deposited in the presence of both H_2O and H_2.

what broader than that observed for films grown using oxygen as the oxidant. Anatase films deposited using oxygen display out-of-plane and in-plane mosaic spreads on the order of 0.1° [35]. This slight degradation in crystallinity does not significantly impact the stabilization of the anatase crystal structure.

In addition to investigating phase dependence on temperature, the effect of water vapor partial pressure on crystallinity was also explored. Fig. 6 shows the X-ray diffraction patterns for films deposited on (001) $LaAlO_3$ at 700 °C with 15 mTorr Ar at a water vapor pressure ranging from 10^{-4} to 10^{-2} Torr. The films deposited at the highest water vapor pressure considered ($P(H_2O) = 10^{-2}$ Torr) were phase-pure anatase with little or no evidence of rutile peaks. At a water vapor pressure of $P(H_2O) = 10^{-4}$ Torr, the phase assemblage changes significantly. Additional peaks in the X-ray diffraction pattern reflect the presence of crystalline Magnéli phases of the type Ti_nO_{2n-1}[37,38]. Given the density of diffraction peaks observed for these triclinic phases, it is not possible to unequivocally identify which phase is present. The most likely candidates are Ti_4O_7 and Ti_6O_{11}. Note that the Magnéli phase(s) displays some degree of preferred texture.

Similar film-growth experiments were performed with sputter deposition occurring in the presence of H_2O and hydrogen. For these experiments, the Ar sputter gas was replaced with a 4%H_2/96%Ar mixture, yielding a H_2 pressure of 6×10^{-4} Torr. The motivation for investigating the effect of hydrogen and H_2O on growth and properties is the possibility of increasing the carrier density in TiO_2 films via oxygen vacancies. In fact, films deposited with H_2O and hydrogen did show an apparent increase in oxygen vacancies, based on dark coloration of the films and increased conductivity. Unfortunately, the introduction of hydrogen also led to mixed-phase films. Fig. 7 shows the X-ray diffraction patterns for TiO_2 films deposited in the presence of both H_2O and H_2. A significant fraction of the rutile phase is observed in the films. The maximum anatase phase density is realized at a deposition temperature of approximately 650 °C. A detailed study of transport properties in semiconducting TiO_2 films are ongoing and will be reported elsewhere.

In addition to crystallinity, we also examined the TiO_2 film morphology for films deposited using H_2O with and without H_2, and compared these to films deposited with oxygen. Atomic force microscopy images of films deposited in O_2, H_2O–H_2, and H_2O clearly indicate a significant change in nucleation and growth when H_2O is used. For the films deposited in O_2, films are extremely smooth, with a root mean square (RMS) roughness of 2.1 nm. With H_2O and H_2O–H_2 ambients, the RMS roughness was 18.5 nm and 30 nm, respectively. For electronic applications, the roughness will significantly limit the utility of films grown using H_2O. For catalysis, the enhanced surface area realized with rough films could prove advantageous. The RMS roughness also increased with increasing deposition temperatures. Fig. 8 shows the RMS roughness, measured with

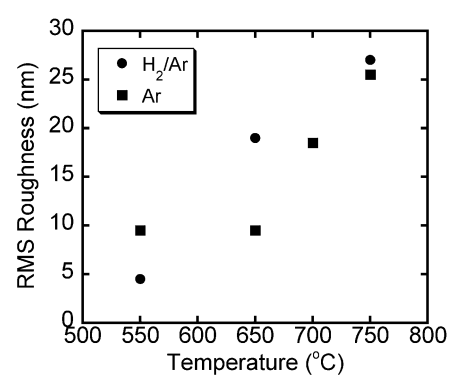

Fig. 8. RMS data for TiO_2 films deposited on $LaAlO_3$ at various substrate temperatures. For these experiments, total pressure was 15 mTorr, RF power was 250 W, and water vapor pressure was 10^{-3} Torr.

AFM, as a function of deposition temperature for films grown by H_2O and H_2O with hydrogen.

In conclusion, we have investigated the epitaxial stabilization of TiO_2 possessing the anatase structure on (001) $LaAlO_3$ using reactive sputter deposition. Phase-pure anatase can be achieved using either water vapor or oxygen as the oxidizing species, although crystallinity was slightly degraded for films grown with water vapor. The use of hydrogen during growth to manipulate Ti valence appears possible, although controlling phase formation remains challenging. Future activities will focus on understanding the electronic, doping, and optical properties of these films.

Acknowledgments

This work was partially supported by the Army Research Office through research grant DAAD 19-01-1-0508 grant. The authors would also like to acknowledge the staff of the Major Analytical Instrumentation Center, Department of Materials Science and Engineering, University of Florida, for their assistance with this work.

References

[1] H.L. Hartnagel, A.L. Dawar, A.K. Jain, C. Jagadish, Semiconducting Transparent Thin Films, Institute of Physics, Bristol, 1995.
[2] H. Meixner, U. Lampe, Sensor. Actuator. B 33 (1996) 198.
[3] A. Rothschild, F. Edelman, Y. Komem, F. Cosandey, Sensor. Actuator. B B67 (2000) 282.
[4] N. Savage, B. Chwieroth, A. Ginwalla, B.R. Patton, S.A. Akbar, P.K. Dutta, Sensor. Actuator. B 79 (2001) 17.
[5] L. Chow, M. Yuen, P. Chan, A. Cheung, Sensor. Actuator. B 76 (2001) 310.
[6] M. Koesch, S. Cassaignon, I. Suillemoles, J.R. Jolivet, Thin Solid Films 403–404 (2002) 312.
[7] M.D. Wiggins, M.C. Nelson, C.R. Aita, J. Vac. Sci. Technol. A 14 (1996) 772.
[8] P. Löbl, M. Huppertz, D. Mergel, Thin Solid Films 251 (1994) 72.
[9] L.-J. Meng, M. Andritschky, M.P. dos Santos, Appl. Surf. Sci. 65–66 (1993) 235.
[10] J.V. Grahn, M. Linder, E. Fredriksson, J. Vac. Sci. Technol. A 16 (1998) 2495.
[11] N. Kaliwoh, J.-Y. Zhang, I.W. Boyd, Appl. Surf. Sci. 186 (2002) 241.
[12] H. Berger, H. Tang, F. Lévy, J. Cryst. Growth 130 (1993) 108.
[13] R. Hengerer, B. Bolliger, M. Erbudak, M. Grätzel, Surf. Sci. 460 (2000) 162.
[14] H. Tang, H. Berger, P.E. Schmid, F. Levy, Solid State Commun. 92 (1994) 267.
[15] H. Tang, K. Prasad, R. Sanjines, P.E. Schmid, F. Levy, J. Appl. Phys. 75 (1994) 2042.
[16] E. Yagi, R.R. Hasiguti, M. Aono, Phys. Rev. B 54 (1996) 7945.
[17] J.W. DeFord, O.W. Johnson, J. Appl. Phys. 54 (1983) 889.
[18] L. Forro, O. Chauvet, D. Emin, L. Zuppiroli, H. Berger, F. Lévy, J. Appl. Phys. 75 (1994) 633.
[19] A. Bernasik, M. Radecka, M Rekas, M. Sloma, Appl. Surf. Sci. 66 (1993) 240.
[20] K.I. Hadjiivanov, D.G. Liissurski, Chem. Soc. Rev. 25 (1996) 61.
[21] A.L. Linsebigler, G. Lu, J.T. Yates, Chem. Rev. 95 (1995) 735.
[22] B. O'Regan, M. Grätzel, Nature 353 (1991) 737.
[23] S. Sato, Shokubai (catalyst) 31 (1989) 469.
[24] Y. Matsumoto, M. Murakami, T. Shono, T. Hasegawa, T. Fukumura, M. Kawasaki, P. Ahmet, T. Chikyow, S. Koshihara, H. Koinuma, Science 291 (2001) 854.
[25] C.K. Ong, S.J. Wang, Appl. Surf. Sci. 185 (2001) 47.
[26] G.S. Herman, Y. Gao, Thin Solid Films 397 (2001) 157.
[27] S. Yamamoto, T. Sumita, Sugiharuto, A. Miyashita, H. Naramoto, Thin Solid Films 401 (2001) 88.
[28] M. Schvisky, K. Kukli, J. Aarik, J. Lu, A. Harsta, J. Cryst. Growth 235 (2002) 293.
[29] T. Miyagi, T. Ogawa, M. Kamei, Y. Wada, T. Yamazaki, E. Ohta, T. Sato, Jpn. J. Appl. Phys. 40 (2001) L404.
[30] P.A. Morris Hotsenpiller, G.A. Wilson, A. Roshko, J.B. Rothman, G.S. Rohrer, J. Cryst. Growth 166 (1996) 779.
[31] M. Murakami, Y. Matsumoto, K. Nakajima, T. Makino, Y. Segawa, T. Chikyow, P. Ahmet, M. Kawasaki, H. Koinuma, Appl. Phys. Lett. 78 (2001) 2664.
[32] Sugiharto, S. Yamamoto, T. Sumita, A. Miyashita, J. Phys.: Condens. Mater. 13 (2001) 2875.
[33] S. Chen, M.G. Mason, H.J. Gysling, G.R. Paz-Pujalt, T.N. Blanton, T. Castro, K.M. Chen, C.P. Fictoe, W.L. Gladfelter, A. Franciosi, P.I. Cohen, J.F. Evans, J. Vac. Sci. Technol. A 11 (1993) 2419.
[34] W. Sugimura, A. Yamazaki, H. Shigetani, J. Tanaka, T. Mitsuhashi, Jpn. J. Appl. Phys. 36 (Pt.1) (1997) 7358.
[35] B.-S. Jeong, J.D. Budai, D.P. Norton, Thin Solid Films 422 (2002) 166.
[36] J.Y. Huang, B.H. Park, D. Jan, X.Q. pan, Y.T. Zhu, Q.X. Jia, Philos. Mag. A 82 (2002) 735.
[37] A. Afir, M. Achour, N. Saoula, J. Alloys Compd. 288 (1999) 124.
[38] Powder Diffraction File, Joint Committee on Powder Diffraction Standards, ASTM, Philadelphia, PA, Cards 18-1401 and 18-1402.